Available online at www.sciencedirect.com
SCIENCE DIRECT®
Journal of the European Ceramic Society 25 (2005) 1619–1627
www.elsevier.com/locate/jeurceramsoc

Properties of liquid phase pressureless sintered silicon carbide obtained without sintering bed

Giuseppe Magnani[a,*], Leandro Beaulardi[b], Luigi Pilotti[a]

[a] *ENEA, Bologna Research Center, Via dei Colli, 16-40136 Bologna, Italy*
[b] *ENEA, Faenza Research Center, Via Ravegnana, 186-48018 Faenza, Italy*

Received 23 July 2003; received in revised form 3 May 2004; accepted 7 May 2004
Available online 16 September 2004

Abstract

High density pressureless sintered silicon carbide bodies with yttria and alumina as sintering aids were obtained without sintering bed (LPSSC-NB). Sintering behavior of this material was studied between 1850 °C and 1950 °C and it was compared to the liquid phase sintered SiC material obtained using sintering bed (LPSSC-B). Sintered density was 97% of the theoretical density (T.D.) at 1875 °C. Mechanical properties like fracture toughness, hardness, flexural strength were determined and compared to other SiC-based materials. In this manner we were able to demonstrate that silicon carbide could successfully be sintered by means of liquid phase mechanism also without sintering bed. This fact opens liquid phase sintered silicon carbide to a wide range of industrial application.

Keywords: Sintering; Mechanical properties; SiC

1. Introduction

Silicon carbide (SiC) is a very interesting ceramic material due to its properties like high hardness, low bulk density, high oxidation resistance which made SiC useful for a wide range of industrial application. Sintering of silicon carbide was first performed by Prochazka[1] by using boron and carbon as sintering aids. These additives allowed to reach high density at temperature over 2000 °C by means of reduction of the superficial energy of the grains (boron)[2] and reaction with residual silica (carbon)[2–4] situated on the SiC particle surface. Using β-SiC instead of α-SiC is more difficult to obtain high density because of at 1900–2000 °C begins transformation β to α which causes porosity entrapping between grains due to the different morphology of β and α grains.[5] In this case, phase transformation could be controlled by using hot-pressing which allowed to reduce sintering temperature, grain growth and thus to enhance mechanical properties.[6] Production of high performance components depends on the good control of microstructure; in fact it is well-known that mechanical properties of ceramic materials is strictly controlled by average grain size.[7] Several additives like Al–C, Al_2O_3–C, and Al_2O_3–Y_2O_3[8–11] were tested as sintering aids for silicon carbide powder to enhance sintering rate and to reduce grain growth. These additives were used instead of boron together carbon or alone (alumina–yttria) and sintering mechanism was already explained for each of these aids; Al[8] and alumina[9] together carbon promoted silicon carbide sintering via solid-state mechanism (SSiC) at temperature over 2000 °C, while alumina and yttria led to high density sintered sample via liquid-phase mechanism (LPSSC) below 2000 °C.[10] The pressureless sintering process based on the densification promoted by a liquid phase (YAG) needs a sintering bed to limit the weight loss associated to the decomposition of alumina and yttria.[11] As an alternative, LPSSC can be obtained with more expensive sintering processes like hot pressing and gas pressure sintering using alumina-yttria or also the AlN–Y_2O_3 system.[12] In any case, liquid phase sintering process does not find up to now a considerable market penetration due to its higher cost than traditional sintering

* Corresponding author.

0955-2219/$ – see front matter © 2004 Elsevier Ltd. All rights reserved.
doi:10.1016/j.jeurceramsoc.2004.05.014

Table 1
Chemical and physical properties of SiC, alumina, and yttria powders

Powder	Purity (wt.%)	Specific surface area (m^2/g)	Particle size (μm)
β-SiC	>97.5	11.59	0.72
Y_2O_3	99.99		3.5–4.3
Al_2O_3	99.99	10	<0.3

process. Our work, reported in this paper, was focused on the characterization of sintered bodies obtained by means of liquid phase pressureless sintering process without using sintering bed in order to demonstrate that liquid phase sintering process can represent a valid alternative to SSiC from mechanical properties and economic evaluation point of views.

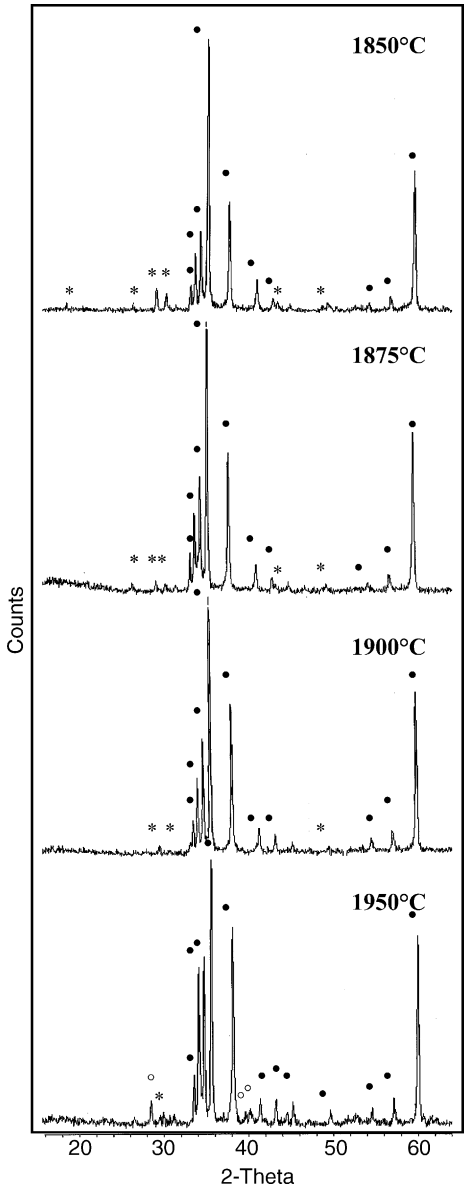

Fig. 1. XRD pattern of the LPSSC-NB samples sintered at 1850 °C, 1875 °C, 1900 °C, and 1950 °C (●, SiC; ✻, YAM ($Y_4Al_2O_9$); ◯, Y_2SiO_5).

2. Experimental procedure

β-SiC powder (BF12, H.C. Starck, Germany) was wet mixed in ethanol with 4 wt.% Y_2O_3 (purity 99.99%, Mandoval Ltd., UK) and 6 wt.% Al_2O_3 (purity 99.99%, Baikalox SM8, Baikowski Chimie France). Characteristics of SiC, alumina and yttria powders are reported in Table 1 . Mixing was performed by Turbula mixer using polyethylene bottle and SiC balls as grinding media. After drying and sieving, the powder was compacted by die pressing at 67 MPa and subsequently was pressed at 250 MPa by CIP.

Green body was put in a graphite crucible without powder bed. Sintering was performed in a graphite elements furnace in flowing Ar at 1 atm. Sintering behavior was investigated in the temperature range 1850–1950 °C. Thermal cycle was characterized by heating and cooling rate of 20–30 °C/min and by dwell time of 0.5 h at sintering temperature. Density of the sintered samples was determined using Archimede's method. Crystalline phases was identified by means of X-ray diffraction (Rigaku-Miniflex Cu Kα: 1.54 Å). Microstructure of pressureless sintered materials was analyzed on fracture, polished, plasma etched (70% CF_4–30% O_2 for 30 min) surfaces, by scanning electron microscopy and microanalysis (Leo 438VP, Leo).

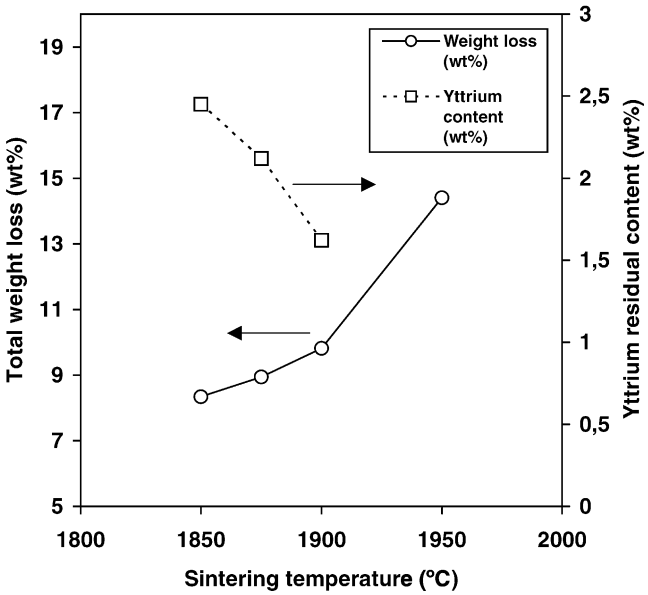

Fig. 2. Weight loss and yttrium residual content as function of the sintering temperature.

Table 2
Variation of YAM content, theoretical density, and sintered density with sintering temperature

Sintering temperature (°C)	YAM content (wt.%)	Theoretical density (g/cm^3)	Sintered density (T.D. %)
1850	3.81	3.24	94.3
1875	3.30	3.23	97.1
1900	2.52	3.22	96.8

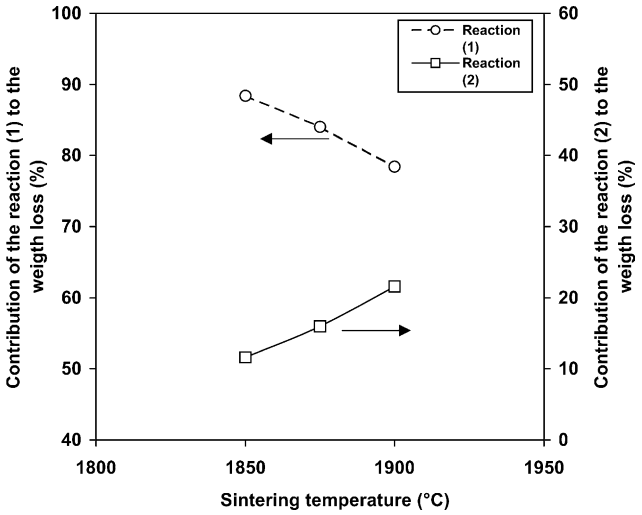

Fig. 3. Contribution of the reactions (1) and (2) to the total weight loss as function of the sintering temperature.

Flexural strength was measured by four-point bend tests at different temperature from RT to 1400 °C. Samples as bars of 2 mm × 2.5 mm × 25 mm were prepared and tested in according to the standard EN 843-1 (crosshead speed: 0.5 mm/min). Fifteen bars for each temperature were tested. Hardness and fracture toughness were determined by means of Vickers indentation method (Durimet-Leitz). Tests were conducted at different load within the range 2.9–196 N (five samples each load). Fracture toughness was calculated using equation proposed by Niihara et al.[13] for median crack:

$$K_{IC} = 0.203\left(\frac{c}{a}\right)^{-3/2} Ha^{1/2} \quad (1)$$

where c is the crack length, a the impression radius and H the hardness.

3. Results and discussion

3.1. Grain boundary phase, density and microstructure

Theoretical density of liquid phase sintered silicon carbide is strictly connected with weight loss. It is well-known that during sintering weight loss is due to the following chemical reactions:[11]

$$SiC(s) + Al_2O_3(s) \Leftrightarrow Al_2O(g) + SiO(g) + CO(g) \quad (1)$$

$$SiC(s) + 2Y_2O_3(s) \Leftrightarrow 4YO(g) + SiO(g) + CO(g) \quad (2)$$

Because of weight loss depends on sintering temperature, theoretical density changes with temperature, too. In order to evaluate the variation of the theoretical density with sintering temperature, secondary phase content had to be determined. First of all, XRD analysis were performed to identify grain

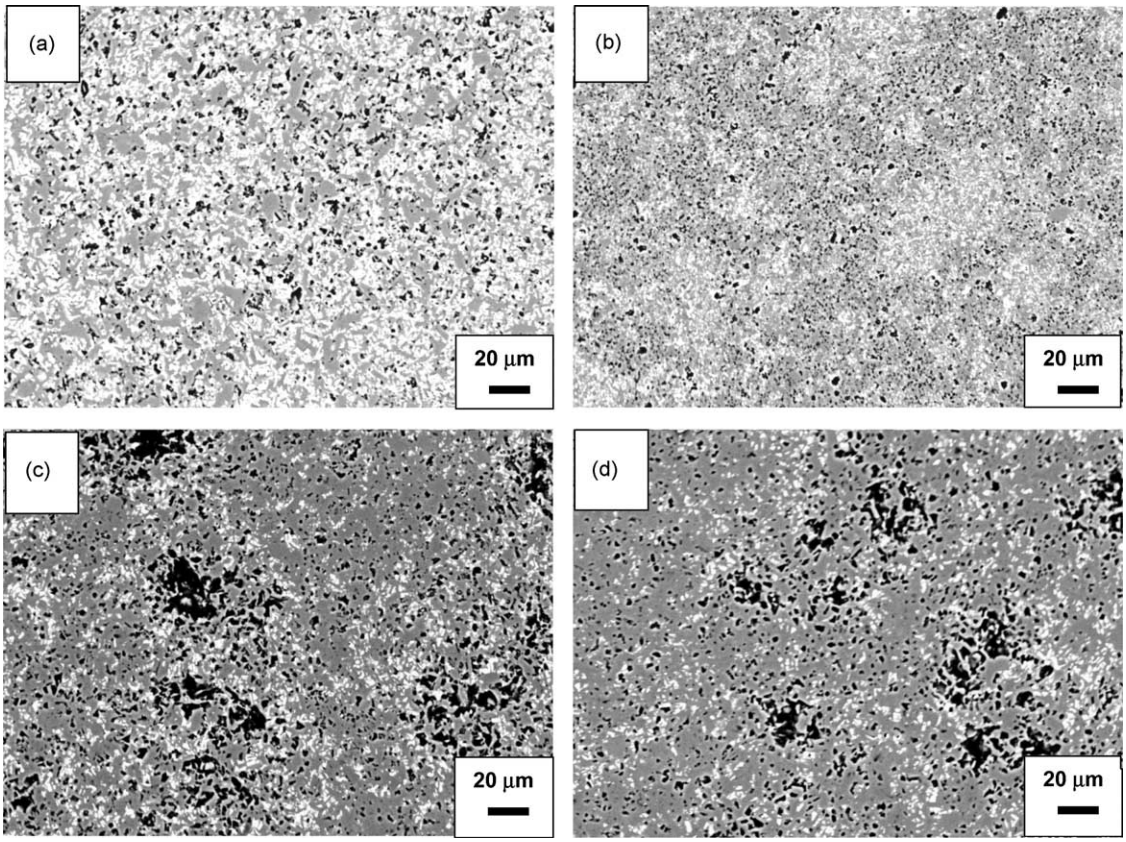

Fig. 4. SEM back-scattered images of the samples sintered at: (a) 1850 °C, (b) 1875 °C, (c) 1900 °C, and (d) 1950 °C.

boundary phase. In Fig. 1 XRD spectra of the samples sintered in the range 1850–1950 °C are reported. The main secondary phase was yttrium aluminate monoclinic ($Y_4Al_2O_9$, YAM) up to 1900 °C, while low amount of yttrium silicate (Y_2SiO_5) was detected together to YAM in the sample sintered at 1950 °C.

This behavior is completely different if it is compared with liquid phase sintered silicon carbide obtained using the powder bed (LPSSC-B). In this case grain boundary phase is composed by yttrium aluminate garnet ($Y_3Al_5O_{12}$, YAG).[11] A possible explanation can be extrapolated on the basis of the weight loss and Al_2O_3–Y_2O_3 phase diagram.[14] In fact, we have already reported that LPSSC-B showed at 1850 °C a total weight loss of 5.2 wt.%,[14] while without sintering bed (LPSSC-NB) the weight loss was 8.3 wt.%. Taking in account the Al_2O_3–Y_2O_3 phase diagram reported by Abell et al.,[15] it is clear that YAM is obtained with a yttria/alumina molar ratio of 2, while YAG is formed when the molar ratio is 0.6. As consequence, YAG was identified as grain boundary phase in LPSSC-B where the starting molar ratio was very close to 0.6. Though LPSSC-NB showed the same initial ratio of LPSSC-B, YAM was detected instead of YAG. This was probably due to the higher weight loss, which led to a strong increasing of the yttria/alumina molar ratio. That means that weight loss was mainly due to the alumina volatilization (reaction (1)) confirming experimental results previously reported by Grande et al.[16] In this manner a yttria/alumina molar ratio close to 2 was achieved and YAM was formed.

For the calculation of the theoretical density, YAM content had to be determined. It was possible through chemical analysis of the yttrium. In fact, yttrium residual content of the sintered samples obtained at different sintering temperature was achieved following analytical method described elsewhere.[14] Analytical results (Fig. 2) put in evidence that yttrium content decreased linearly when sintering temperature is raised.

On the basis of these analysis, YAM content and theoretical density could be calculated. Results are reported in Table 2 together with the sintered density. Theoretical density was calculated following the mixture's rule with 4.52 g/cm^3 as YAM bulk density and 3.2 g/cm^3 for SiC. The sintered density reached the maximum value at 1875 °C (97 T.D.%), whereas at 1900 °C the higher weight loss (10 wt.%) led to a decreasing of the liquid phase content, which, limiting the solution–precipitation process, reduced the densification. Therefore, the densification is hindered when the total weight loss is higher than 9 wt.%. This is in good agreement with previous study where a maximum density of only 87% T.D. was obtained without using powder bed.[16] Furthermore, the same authors demonstrated the approximately one third to one half of the alumina content in the sintering sample was removed and that the overall composition of the secondary

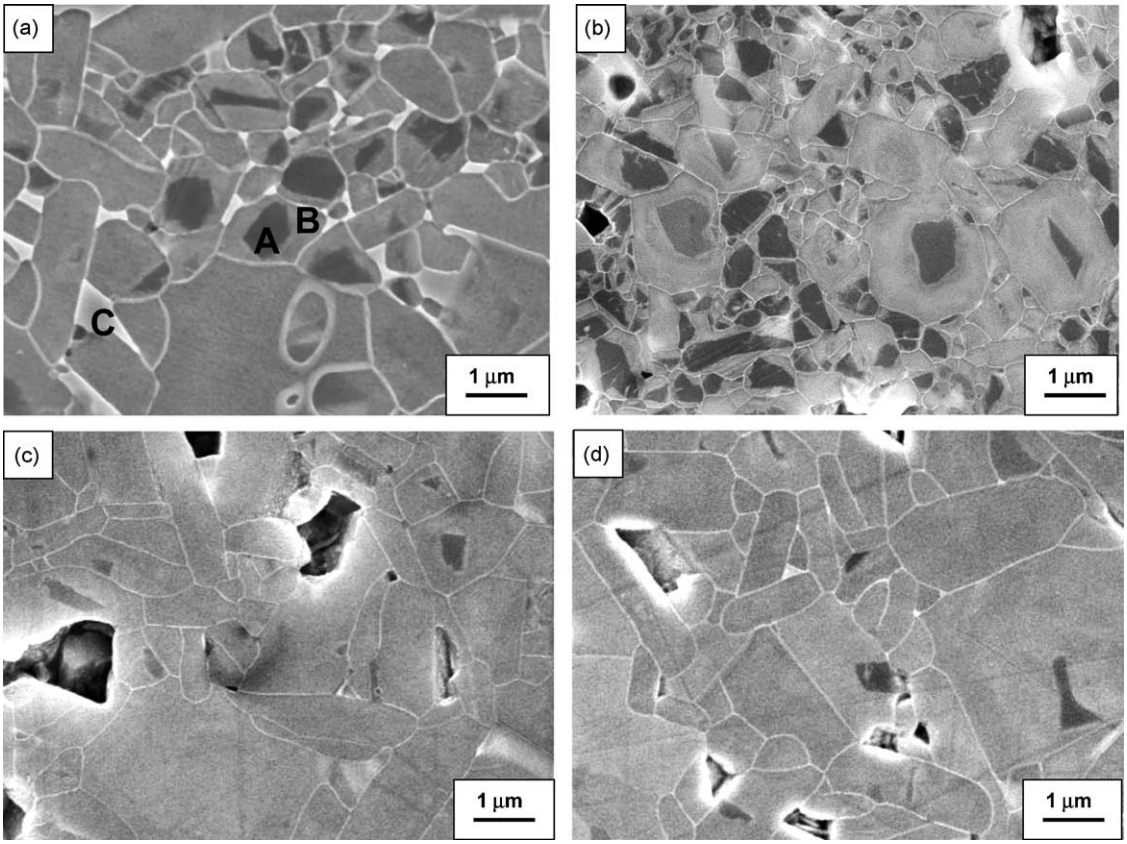

Fig. 5. SEM of the plasma etched samples sintered at: (a) 1850 °C, (b) 1875 °C, (c) 1900 °C, and (d) 1950 °C.

phase deviated considerably from the initial eutectic composition. We propose the same conclusions on the basis of the experimental observations. In addition, we were also able to calculate accurately the contribution of the reactions (1) and (2) to the total weight loss associated to the sintering. This calculation confirmed quantitatively that alumina decomposition is the main contribution to the weight loss (88% at 1850 °C). As reported in Fig. 3, it decreased with increasing sintering temperature up to reach the value of 78% at 1900 °C.

As a consequence of the reactions (1) and (2), residual porosity was detected inside the sintered samples. Fig. 4a–d clearly show that weight loss led to a homogeneously distributed fine porosity at 1850–1875 °C, while samples sintered at higher sintering temperature (>1900 °C) showed large voids which are able to compromise fracture and oxidation resistance. Additional microstructural investigations were performed after plasma etching (Fig. 5a–d). The method of plasma etching has mainly been used for Si-based compounds (Si_3N_4, SiAlON, SiC) and it is particularly indicated for liquid phase sintered ceramics. Etched surfaces of LPSSC-NB samples revealed a core–rim structure in SiC grains more pronounced at low sintering temperature (<1900 °C) due to the higher grain boundary phase content. EDS analysis of the core–rim structure are reported in Fig. 6a–c. In the core region (point A in Fig. 5a) only Si and C were detected, whereas Si, Al and Y could be revealed in the rim (point B). This provided evidence that liquid phase sintering of SiC proceeded via a classical solution and re-precipitation mechanism with Al_2O_3–Y_2O_3 additive systems that during densification and grain growth formed a reactive

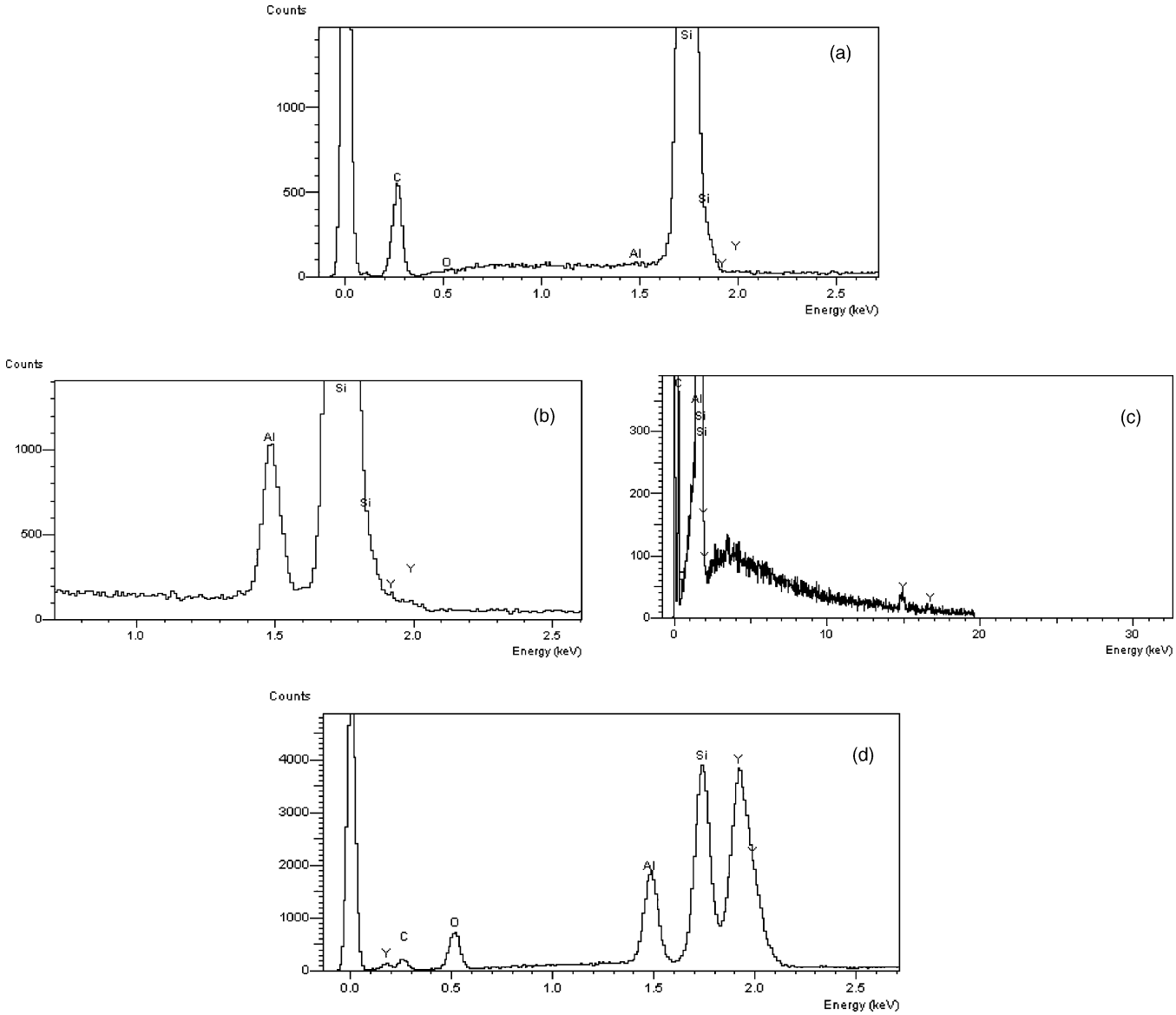

Fig. 6. EDS patterns of: (a) core of the SiC grains (point A in Fig. 5a), (b) $Si_{L\alpha}$ and $Al_{L\alpha}$ in the rim of the SiC grains, (point B), (c) $Y_{K\alpha}$ in the rim of the SiC grains (point B), and (d) grain boundary phase (point C).

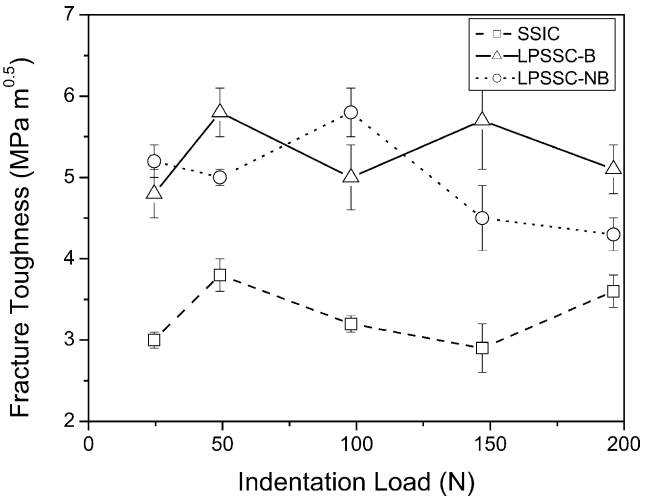

Fig. 7. Fracture toughness of LPSSC-NB, LPSSC-B, and SSiC at different indentation load.

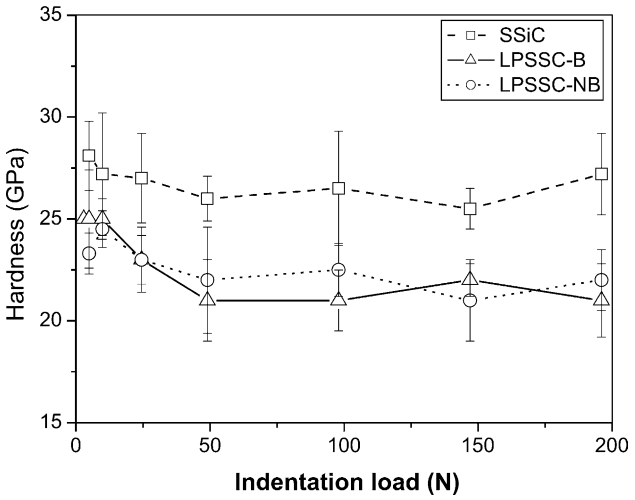

Fig. 8. Vickers hardness of LPSSC-NB, LPSSC-B, and SSiC at different indentation load.

Al–Y–O rich liquid phase.[17] This phase (YAM) is indicated with point C in Fig. 5a and its EDS spectra is reported in Fig. 6c.

3.2. Mechanical properties

Evaluation of mechanical properties of LPSSC-NB materials sintered at 1875 °C was made in comparison with two types of SiC-based materials manufactured by ourselves: LPSSC-B with alumina and yttria as additives system and sintered silicon carbide (SSiC) with boron and carbon as sintering aids. Fracture toughness and hardness values as a function of the indentation load are reported in Figs. 7 and 8, respectively. Fracture toughness did not show any difference between LPSSC-B and LPSSC-NB, while SSiC showed the lowest values (Fig. 7). Microstructural investigation confirmed that the higher fracture toughness in LPSSC-NB is mainly due to the crack deflection mechanism (Fig. 9), as it was already demonstrated in LPSSC-B.[18] On the contrary, SSiC presented the highest hardness, while LPSSC-NB and LPSSC-B showed more or less the same values. It can also be noticed that the measured hardness decreases with an increase in load and at high indentation load (>50 N), hardness–load curves for all three SiC-based materials flatten out and hardness became constant. This is a well-know phenomenon of ceramic materials[19] called indentation size effect (ISE) which can be analyzed using different models proposed for macro-, micro- and nanoindentation.[20,21] Examining the curves reported in Fig. 8, it is evident that the ISE at low loads appears nearly linear in all three materials prior to a constant hardness transition, H_C, which it is normally linked to the fracture toughness. In fact, previous studies demonstrated that H_C is higher in the materials having low fracture toughness.[20] It was also confirmed in our case where H_C was 26.5, 21, 21 GPa in SSiC, LPSSC-B, and LPSSC-NB, respectively.

Finally, LPSSC-NB was compared with the other SiC-based materials from the flexural strength point of view. SSiC material is already known for its high oxidation resistance at

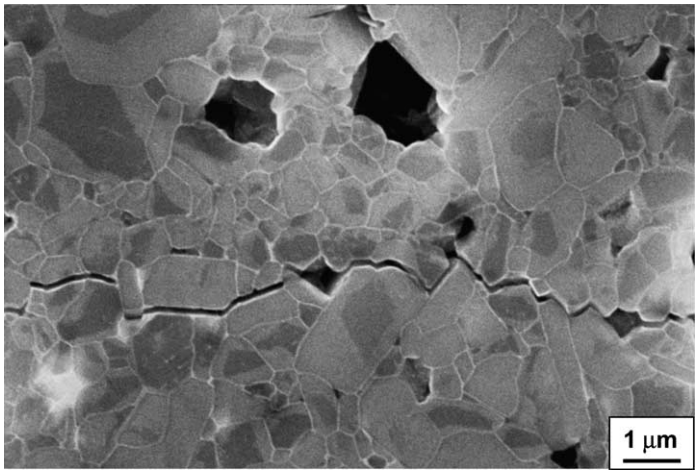

Fig. 9. SEM image of the crack propagation in LPSSC-NB materials.

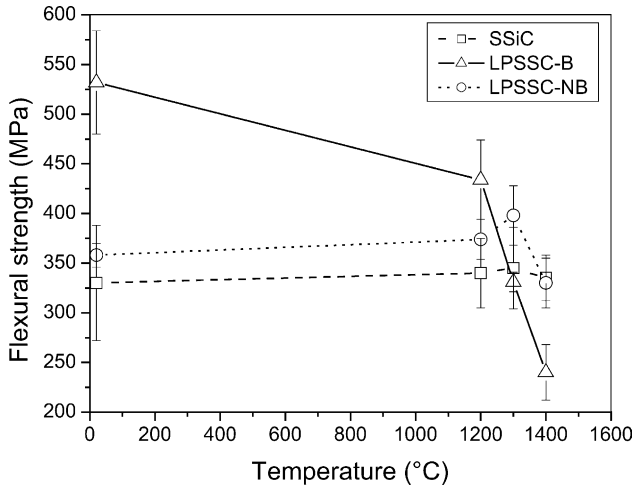

Fig. 10. Variation of the flexural strength of LPSSC-NB, LPSSC-B, and SSiC with temperature.

high temperature, whereas it is also known that LPSSC-B shows a good oxidation resistance only up to 1200 °C due to the formation of a superficial glassy phase containing large pores and holes.[11] Behaviour of LPSSC-NB ceramics is quite different if it is compared to the other SiC-based materials (Fig. 10). At room temperature LPSSC-NB exhibited a lower bending strength than LPSSC-B (358 and 532 MPa, respectively). It was probably due to the higher weight loss in LPSSC-NB materials, which could increment number and size of the critical defects. SEM analysis of the fracture surface revealed that the fracture origin could sometimes be found in correspondence of these defects (Fig. 11). Nevertheless, the reliability of this material can be considered good if the scatter in the measured strength is taken in account as reliability's index (Fig. 10). At high temperature, flexural strength of LPSSC-NB was still higher than 300 MPa (398 MPa at 1300 °C and 330 MPa at 1400 °C) confirming its high oxidation resistance. On the contrary, LPSSC-B started to present a strong reduction of its oxidation resistance already at 1200 °C. More informations about the different high temperature behavior between LPSSC-NB and

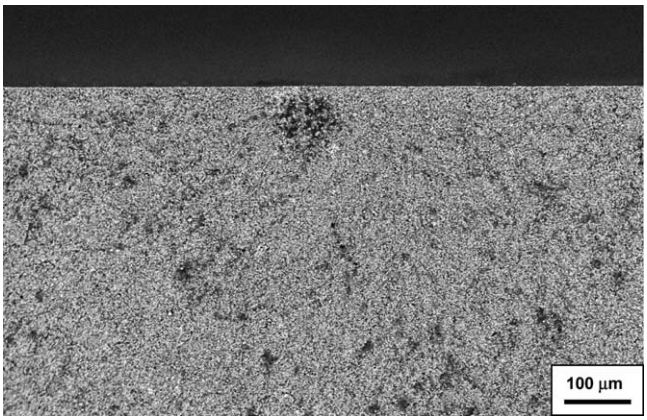

Fig. 11. Critical defect in a bar tested at room temperature.

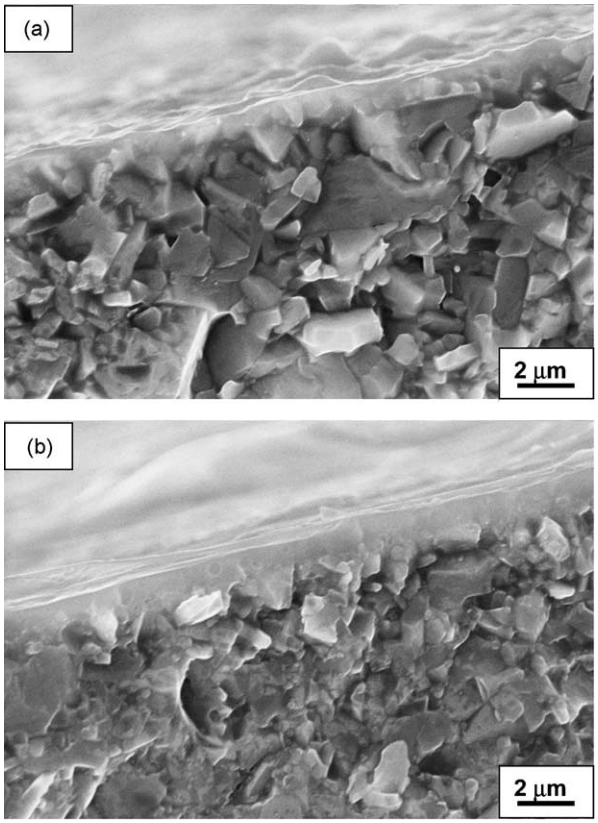

Fig. 12. SEM image of the fracture surface of LPSSC-NB sample tested at (a) 1300 °C and (b) 1400 °C.

LPSSC-B were achieved by means of the SEM analysis of fracture surface of the samples tested at 1300 °C and 1400 °C. We have already demonstrated that LPSSC-B samples tested at 1400 °C showed a superficial layer of γ-$Y_2Si_2O_7$ which contained large pores and holes that did not protect sintered samples from oxygen diffusion. On the contrary, LPSSC-NB formed an oxidation scale (Fig. 12a and b) that did not show any defects, and therefore, acted as protective layer at high temperature. Furthermore, its thickness increased from 2 μm at 1300 °C (Fig. 12a) up to 4 μm at 1400 °C (Fig. 12b) ensuring a strong barrier against oxygen diffusion. Identification of the crystalline phases contained in the oxidation scale was performed by means of XRD analysis (Fig. 13a and b). YAG ($Y_3Al_5O_{12}$), SiO_2 (α-cristobalite) and γ-$Y_2Si_2O_7$ (yttrium disilicate) were identified as main oxidation species at 1300 °C, while only α-cristobalite and yttrium disilicate were found in the sample tested at 1400 °C. This behavior can be explained on the basis of the chemical reactions reported in Table 3. At 1300 °C, yttrium aluminate monoclinic (YAM) reacts with silica (oxidation product of SiC) to form yttrium aluminate garnet (YAG), yttrium silicate and a small amount of alumina. Increasing the temperature up to 1400 °C, YAG and silica reacts together to form yttrium disilicate and alumina as by-product. In both cases, free alumina was not detected with XRD analysis due to its very low content.

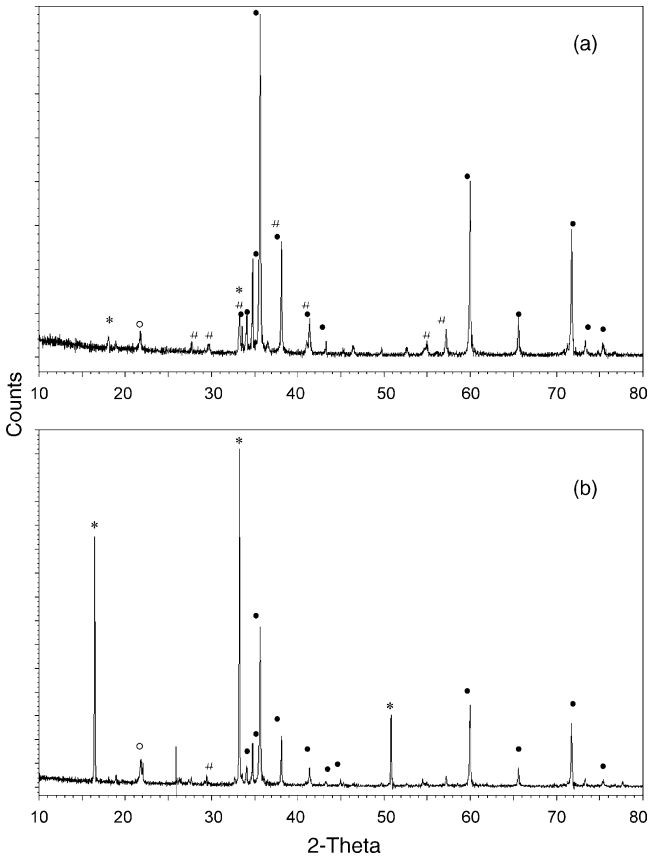

Fig. 13. XRD pattern of LPSSC-NB sample tested at (a) 1300 °C and (b) 1400 °C (●, SiC; ✻, γ-$Y_2Si_2O_7$; ◯, α-cristobalite SiO_2; ⫽, YAG).

In general, these experimental results confirms that γ-$Y_2Si_2O_7$ is the favorite phase at temperature higher than 1300 °C.[22] Furthermore, the formation of a superficial layer of yttrium disilicate is promising from creep resistance point of view on the basis of the studies conducted by Schneider et al.[12] In fact, they have already demonstrated that liquid-phase sintered silicon carbide obtained by gas pressure sintering with AlN–Y_2O_3 as additive system shows a good creep resistance at 1400 °C due to the development of a low viscosity liquid phase, γ-$Y_2Si_2O_7$. This fact together to the high oxidation resistance make pressureless liquid phase sintering without powder bed a suitable process for the production of silicon carbide components for applications at high temperature.

Table 3
High temperature reactions in oxidizing environment for LPSSC-NB materials

1300 °C
$SiC(s) + \frac{3}{2}O_2(g) \Leftrightarrow SiO_2(s) + CO(g)$
$14SiO_2(s) + 5Y_4Al_2O_9(s) \Leftrightarrow 7Y_2Si_2O_7(s) + 2Y_3Al_5O_{12}(s)$
$4SiO_2(s) + Y_4Al_2O_9(s) \Leftrightarrow 2Y_2Si_2O_7(s) + Al_2O_3(s)$
1400 °C
$SiC(s) + \frac{3}{2}O_2(g) \Leftrightarrow SiO_2(s) + CO(g)$
$6SiO_2(s) + 2Y_3Al_5O_{12}(s) \Leftrightarrow 3Y_2Si_2O_7(s) + 5Al_2O_3(s)$

4. Conclusion

We have demonstrated that silicon carbide can be pressureless sintered using yttria and alumina as sintering aids and without sintering bed. YAM was detected as grain boundary phase instead of YAG due to the higher weight loss. Nevertheless, sintered density reached the value of 97 T.D.% at 1875 °C. Furthermore, this material exhibits high fracture toughness and high oxidation resistance up to 1400 °C that makes it potentially promising for a wide range of applications also at high temperature.

Acknowledgment

Authors wish to thank Dr. F. Monteverde and Sig. A. Balbo (CNR-ISTEC Faenza, Italy) for the plasma etching.

References

1. Prochazka S. *Hot Pressed Silicon Carbide*. US Patent 3853566, 10 December 1974.
2. Maddrell, E. R., Pressureless sintering of silicon carbide. *J. Mater. Sci. Lett.*, 1987, **6**, 486–488.
3. Van Rijswjk, W. and Shanafield, D. J., Effects of carbon as a sintering aid in silicon carbide. *J. Am. Ceram. Soc.*, 1990, **73**(1), 148–149.
4. Hamminger, R., Carbon inclusions in sintered silicon carbide. *J. Am. Ceram. Soc.*, 1989, **72**(9), 1741–1744.
5. Williams, R. M., Juterbock, B. N., Peters, C. R. and Whalen, T. J., Forming and sintering behavior of B- and C-doped α- and β-SiC. *J. Am. Ceram. Soc.*, 1984, **67**(4), C62–C64.
6. Larker, H. T., Hermasson, L. and Adlerborn, J., Hot isostatic pressing and its applicability to silicon carbide and boron carbide. In *High Tech Ceramics—Proceedings of 6th CIMTEC*, ed. P. Vincenzini. Elsevier Science Publishers B.V., Amsterdam, 1987, pp. 795–803.
7. Rice, R. W., Strength–grain size behavior of ZrO_2 at room temperature. *J. Mater. Sci. Lett.*, 1994, **13**, 1408–1412.
8. Stutz, D. H., Prochazka, S. and Lorenz, J., Sintering and microstructure formation of β-silicon carbide. *J. Am. Ceram. Soc.*, 1985, **68**(9), 479–482.
9. Sakai, T., Watanabe, H. and Aikawa, T., Effects of carbon on phase transformation of β-SiC with Al_2O_3. *J. Mater. Sci. Lett.*, 1987, **6**, 865–866.
10. Omori, M. and Takei, H., Preparation of pressureless-sintered SiC–Y_2O_3–Al_2O_3. *J. Mater. Sci.*, 1988, **23**, 3744–3749.
11. Magnani, G., Minoccari, G. L. and Plotti, L., Flexural strength and toughness of liquid phase sintered silicon carbide. *Ceram. Int.*, 2000, **26**, 495–500.
12. Schneider, J., Biswas, K., Rixecher, G. and Aldinger, F., Microstructural changes in liquid-phase-sintered silicon carbide during creep in an oxidizing environment. *J. Am. Ceram. Soc.*, 2003, **86**(3), 501–507.
13. Niihara, K., Nakahira, A. and Hirai, T., The effect of stoichiometry on mechanical properties of boron carbide. *J. Am. Ceram. Soc.*, 1984, **67**, 13–15.
14. Magnani, G., Pilotti, L. and Ronconi, G., Variation of theoretical density with sintering temperature in liquid phase sintered silicon carbide. In *Advances in Science and Technology, Vol 14, Ceramics: Getting into the 2000's—Part B*, ed. P. Vincenzini. Techna, Faenza, 1999, pp. 783–791.
15. Abell, J. S., Harris, I. R., Cockayne, B. and Lent, B., An investigation of phase stability in the Y_2O_3–Al_2O_3 system. *J. Mater. Sci.*, 1974, **9**, 527–537.

16. Grande, T., Sommerset, H., Hagen, E., Wiik, K. and Einarsrud, M. A., Effect of weight loss on liquid-phase sintered silicon carbide. *J. Am. Ceram. Soc.*, 1997, **80**(4), 1047–1057.
17. Sigl, L. S. and Kleebe, H. J., Core rim structure of liquid-phase-sintered silicon carbide. *J. Am. Ceram. Soc.*, 1993, **76**(3), 773–776.
18. Do-Hyeong, K. and Chong Hee, K., Toughening behavior of silicon carbide with additions of yttria and alumina. *J. Am. Ceram. Soc.*, 1990, **73**(5), 1431–1434.
19. Clinton, D. J. and Morrell, R., Hardness testing of ceramic materials. *Mater. Chem. Phys.*, 1987, **17**, 461–473.
20. Quinn, J. B. and Quinn, G. D., Indentation brittleness of ceramics: a fresh approach. *J. Mater. Sci.*, 1997, **32**, 4331–4346.
21. Peng, Z., Gong, J. and Miao, H., On the description of indentation size effect in hardness testing for ceramics: Analysis of the nanoindentation data. *J. Eur. Ceram. Soc.*, 2004, **24**, 2193–2201.
22. Kolitsch, U., Seifert, H. J., Ludwig, T. and Aldinger, F., Phase equilibria and crystal chemistry in the Y_2O_3–Al_2O_3–SiO_2 system. *J. Mater. Res.*, 1999, **14**(2), 447–455.